Rock Mech. Rock Engng. (2004) 37 (1), 25–56
DOI 10.1007/s00603-003-0014-z

Rock Mechanics and Rock Engineering
Printed in Austria

Micromechanical Model for Simulating the Fracture Process of Rock

By

W. C. Zhu and **C. A. Tang**

Center for Rock Instability and Seismicity Research,
Northeastern University, Shenyang, P.R. China

Received March 25, 2003; accepted June 17, 2003
Published online November 6, 2003

Summary

A micromechanical model is proposed to study the deformation and failure process of rock based on knowledge of heterogeneity of rock at the mesoscopic level. In this numerical model, the heterogeneity of rock at the mesoscopic level is considered by assuming the material properties in rock conform to the Weibull distribution. Elastic damage mechanics is used to describe the constitutive law of meso-level elements, the finite element method is employed as the basic stress analysis tool and the maximum tensile strain criterion as well as the Mohr-Coulomb criterion is utilized as the damage threshold. A simple method, similar to a smeared crack model, is used for tracing the crack propagation process and interaction of multiple cracks. Based on this model, a numerical simulation program named Rock Failure Process Analysis Code (RFPA) is developed. The influence of parameters that include the Weibull distribution parameters, constitutive parameters of meso-level elements and number of elements in the numerical model, are discussed in detail. It is shown that the homogeneity index is the most important factor to simulate material failure with this model. This model is able to capture the complete mechanical responses of rock, which includes the crack patterns associated with different loading stages and loading conditions, localization of deformation, stress redistribution and failure process. The numerical simulation of rock specimens under a variety of static loading conditions is presented, and the results compare well with experimental results.

Keywords: Damage mechanics, rock, fracture process, heterogeneity, mesoscopic.

1. Introduction

In recent years, there has been growing interest in numerically modeling the fracture process of rock. Efforts in this direction are very necessary for knowing the fracture mechanism and improving analysis capabilities of the numerical method for engineering use. Observations of internal and external structures of rock provided a better understanding of its failure behavior. It is generally accepted that the deformation of

rock is associated with very complicated progressive failures, as characterized by initiation, propagation, and coalescence of microcracks (Bobet and Einstein, 1998; Eberhardt et al., 1999). In the past, most material characterizations were based on the approximation of representing the rock by one of the classical mathematical models such as elasticity, plasticity and viscoelasticity to describe the nonlinearity of rock. The numerical methods such as finite element method, discrete element method, boundary element method and displacement discontinuity method are also applied to modeling the deformation and fracture of rock (Aliabadi, 1999). One of the most important factors affecting the mechanical behavior during the failure process is the heterogeneity of rock. Linear elastic fracture mechanics provides the basic tools today for the analysis of many solid mechanics problems dealing with crack propagation. However, linear fracture mechanics theory is only applicable to homogeneous materials with a single crack or multiple regular-arrayed cracks, not sufficient to describe the fracture process of heterogeneous quasi-brittle materials such as rock, concrete and ceramics (Carpinteri et al., 1997).

In the research of deformation and failure of rock, microfracturing and crack growth are at the heart of the problem. Micromechanics provides a general framework to solve the fracture of heterogeneous materials such as rock and concrete (Nemat-Nasser and Hori, 1993). In the past, many numerical models that consider the influence of microcracks were developed (Chudnowski and Kunin, 1987; Ortiz, 1988; Myer et al., 1992). Most of these models were based on combining the theory of fracture mechanics or damage mechanics with some statistical treatment to account for the random distribution of microcracks. Because many parameters, such as crack density, must be used to quantify the crack distribution in theses models, they are often difficult to implement in a numerical code (Homand-Etienne et al., 1998).

As pointed out by Van Mier (1997), the different structural features that can be found in a material at a given level of observation can be explained in terms of material structures at a lower level. Therefore, we deem that numerical simulation of the fracture process of rock and other quasi-brittle materials can be carried out at lower level, i.e. the mesoscopic level, at which heterogeneous material properties can be incorporated in the numerical model. With the development of more powerful computational tools and computer techniques it has become possible to simulate the mechanical behavior at such a level that at least part of the internal material structure (such as mesoscopic structures) can be incorporated in the model. Using numerical models to explain the observed failure characteristics of rock is becoming more and more feasible based on successful micromechanical models as computer power increases. For example, the non-linear rule-based model (Blair and Cook, 1998), the lattice model (Chiaia et al., 1997; Van Mier, 1997) and the bonded particle model (Potyondy and Cundall, 1996; Hazzard and Young, 2000) are found to be appropriate to simulate the fracture process of quasi-brittle materials such as rock and concrete. In these models, different methods are used to characterize the randomness and heterogeneity of material at the mesoscopic level, but all these studies follow the same objective of analyzing the influence of mesoscopic internal structures on macroscopic mechanical response. In this investigation, a micromechanical model that can simulate the failure process of rock subjected to variety of plane stress conditions is proposed and validated. Based on this model, a Rock Failure Process Analysis (RFPA) Code is

developed, which had been introduced by Tang in many papers (Tang, 1997; Tang and Kaiser, 1998; Tang et al., 2000).

The RFPA model has been successfully used to simulate failure of rock under a variety of loading conditions, but no detailed description of its constitutive law is given in previous papers (Tang, 1997; Tang and Kaiser, 1998; Tang et al., 2000). In this paper the constitutive law of this model is proposed based on elastic damage mechanics, and is validated by studying the failure of rock specimens subjected to a variety of loading conditions. At first, the heterogeneity of rock is considered by assuming that its mechanical properties, such as Young's modulus and uniaxial compressive strength, conform to the Weibull distribution, so the mechanical parameters of every element are specified stochastically according to the given Weibull distribution parameters. Then, an elastic damage-based constitutive relationship for each mesoscopic element is proposed, and the manner in which the parameters in this constitutive relationship affect the macroscopic load-displacement response is comprehensively discussed. The implementation of this micromechanical model in numerical simulation is briefly described.

2. The Principle of the Numerical Model

It is generally known that the progressive degradation of material properties results from the initiation, growth and coalescence of microcracks. Numerical simulation of fracture processes must reflect the progressive degradation of material subjected to loading. Here the failure process simulation is attained using FEM as the basic stress analysis tool, where the four-node isoparametric element is used as the basic element in the finite element mesh, and the elastic damage-based constitutive relationship of meso-level elements is incorporated. The mechanical parameters of rock, such as Young's modulus, strength and Poisson's ratio, are heterogeneous and assumed to conform to the Weibull distribution. This kind of randomness, used in the assignment of mechanical properties of elements, is quite different from that of the stochastic finite element method (Ostoja-Starzewski, 1993), because the mechanical and geometrical parameters of an element are actually definite after the assignment is finished, and no probability is incorporated in the finite element analysis. The mesoscopic element is assumed to be homogeneous and isotropic, and its damage evolution conforms to the specific elastic damage constitutive law.

2.1 Assignment of Material Properties

In order to capture the heterogeneity of rock at the meso-level, its mechanical parameters, including the Young's modulus, strength and Poisson's ratio, are assumed to conform to the Weibull distribution, as defined by the following probability density function:

$$f(u) = \frac{m}{u_0}\left(\frac{u}{u_0}\right)^{m-1} \exp\left(-\frac{u}{u_0}\right)^{m}, \tag{1}$$

where u is the parameter of the element (such as strength or elastic modulus); the scale parameter u_0 is related to the average of element parameter and the parameter m

defines the shape of the distribution function. The parameter m defines the degree of material homogeneity and is called the homogeneity index. According to the definition of the Weibull distribution, the value of parameter m must be larger than 1.0. Then, we can numerically produce a heterogeneous material in a computer simulation for a material composed of many mesoscopic elements. Here, this heterogeneous material produced by computer is used to simulate the real specimen used in the laboratory, so it is called numerical specimen in this investigation.

Figure 1 shows three numerical specimens, which are all composed of 100×100 elements, produced randomly by computer according to the Weibull distribution with different homogeneity indices. The stochastic distribution of element strengths is also given in Fig. 2. In Fig. 1 the different gray colors correspond to different magnitude of element strengths. It is found that the element strengths are concentrated more closer to u_0 as the homogeneity index increases. So an increase in homogeneity index leads to more homogeneous numerical specimens. In general, we assumed that Young's modulus and strength conform to two individual distributions with the same heterogeneity index. The distribution of Poisson's ratio is not quite narrow in reality; therefore, a high homogeneity index of 100 is specified in the following simulations. The mean value of Poisson's ratio is specified according to real values obtained from laboratory tests. The way in which the homogeneity index affects the macroscopic mechanical response will be discussed in detail later.

Here the mesoscopic elements that are used to represent the heterogeneity of rock are also utilized as the elements in the finite element analysis. The mesoscopic elements are assumed to be isotropic and homogeneous. The elements in the specimen must be relatively small to reflect the mesoscopic mechanical properties of materials, subject to the condition that current computers can perform out the analysis. This probably distribution as defined in Eq. (1) actually reflects the true heterogeneity of material in two respects: first, with different distribution parameters, such as m, different distributions of material properties are represented. Second, with the same distribution parameter, the material properties may be spatially stochastic, that is to say, the properties of every simulated element may be different each time, even if the same Weibull distribution is adopted. In the following part, the effect of these two kinds of heterogeneity will be discussed.

2.2 Constitutive Relations of Element

Continuum damage mechanics has proved to be an efficient tool for the understanding and the description of material evolution. Here we use it to describe the mechanical behavior of mesoscopic elements that describe the rock specimen. In this paper, the material is analyzed at mesoscopic level, by assuming that each element corresponds to the mesoscopic scale. Initially, elements are considered to be elastic; their elastic properties are defined by Young's modulus and Poisson's ratio. The stress-strain curve of each element is considered linear elastic until the given damage threshold is attained. We choose the maximum tensile strain (or stress) criterion and the Mohr-Coulomb criterion, respectively as the damage thresholds. The tensile strain criterion is used primarily to determine whether the element is damaged or not. If the element is

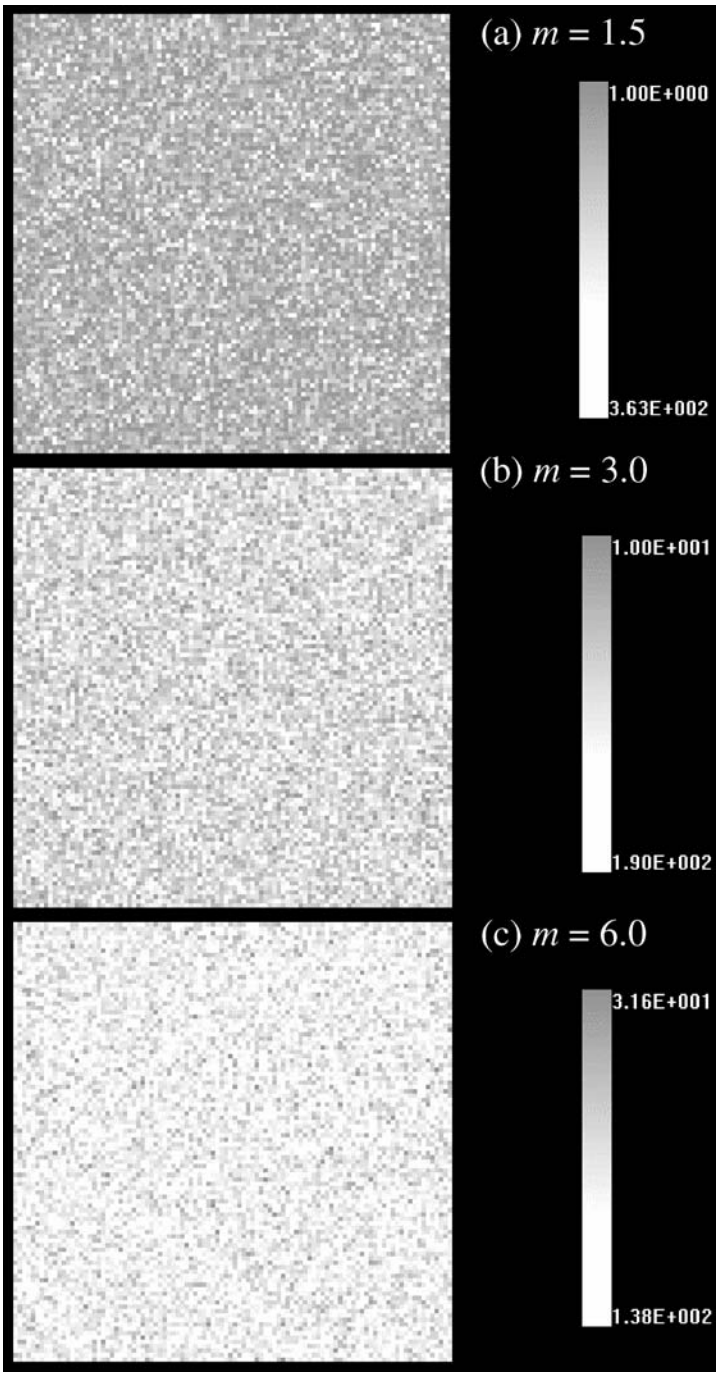

Fig. 1. Distribution of strength of specimens with different homogeneity index. The gray degree in the figure denotes the magnitude of strength of elements

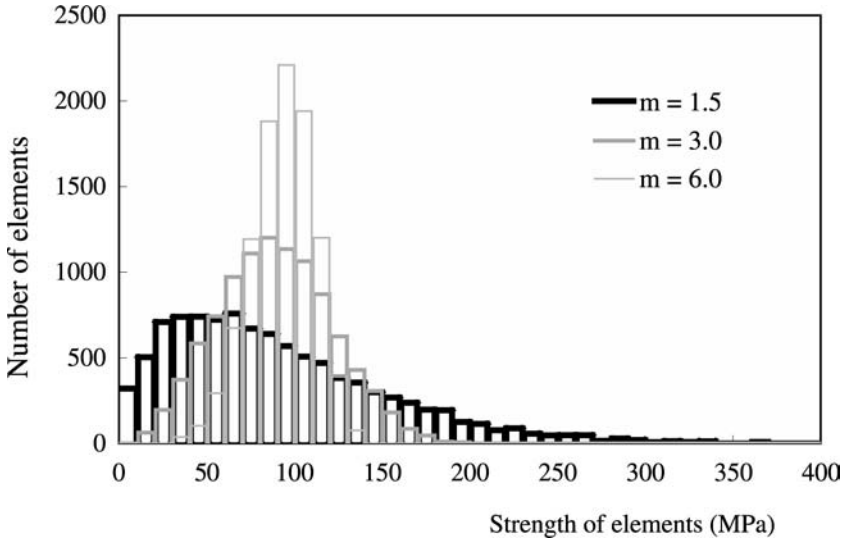

Fig. 2. Histogram of strength of elements in numerical specimens with different homogeneity index (Weibull parameter u_0 is 100 MPa)

not damaged in tensile mode, the Mohr-Coulomb criterion is then used to judge whether the element damage occurs in tensile modes.

2.2.1 Constitutive Law of Mesoscopic Element Damaged in Tensile Mode

When the mesoscopic element is under uniaxial tension, the constitutive relationship illustrated in Fig. 3 is adopted. Fig. 3a presents the elasto-brittle damage constitutive relations with given specific residual strength, while Fig. 3b proposes a damage constitutive law with power function softening in the post-peak region.

In elastic damage mechanics, the stiffness of elements degrades gradually as damage progresses, the elastic modulus of damaged material being defined as follows:

$$E = (1 - D)E_0, \tag{2}$$

where D represents the damage variable, and E and E_0 are elastic moduli of the damaged and the undamaged material, respectively. Here the element and its damage are assumed isotropically elastic, so the quantities E, E_0 and D are all scalars. A total rather than incremental form is used for the proposed constitutive law.

The damage variable D ranges from zero for the undamaged material to one representing the failure. In this study, two kinds of softening curves, as shown in Fig. 3, are used to reflect the softening process under uniaxial tension in order to study how these softening schemes affect the numerical results. Since no initial damage is incorporated in this model, the initial stress-strain curve is linear elastic, thus no damage occurs, i.e. $D = 0$. When the maximum tensile strain criterion is met, element damage occurs. This kind of damage is called tensile damage. The sign

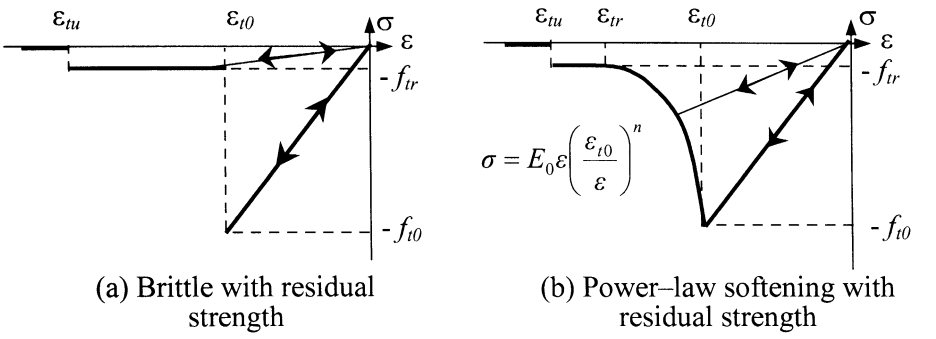

Fig. 3. Elastic damage constitutive law of elements under uniaxial tensile stress (f_{t0} and f_{tr} are uniaxial tensile strength and residual uniaxial tensile strength of element, respectively)

convention used through out this paper is that compressive stresses and strains are positive. For the two softening schemes, different expressions for the damage variable D may be obtained.

With regard to the constitutive law shown in Fig. 3a, the parameter D can be calculated as

$$D = \begin{cases} 0 & \varepsilon > \varepsilon_{t0} \\ 1 - \dfrac{f_{tr}}{E_0 \varepsilon} & \varepsilon_{tu} < \varepsilon \leq \varepsilon_{t0} \\ 1 & \varepsilon \leq \varepsilon_{tu}, \end{cases} \tag{3}$$

where f_{t0} and $\lambda = f_{tr}/f_{t0}$ are the uniaxial tensile strength and the residual strength coefficient, respectively. The residual strength coefficient λ is defined as the ratio between residual strength and initial strength of the element. ε_{t0} is the strain at the elastic limit, which is the so-called threshold strain for tensile damage, while ε_{tu} is the ultimate tensile strain, at which the element would be completely damaged in tensile mode. The ultimate tensile strain is defined by $\varepsilon_{tu} = \eta \varepsilon_{t0}$, where η is called ultimate strain coefficient. Herein f_{tr} is the residual tensile strength, which is given as $f_{tr} = \lambda f_{t0} = \lambda E_0 \varepsilon_{t0}$. Then, the above Eq. (3) can be expressed as

$$D = \begin{cases} 0 & \varepsilon > \varepsilon_{t0} \\ 1 - \dfrac{\lambda \varepsilon_{t0}}{\varepsilon} & \varepsilon_{tu} < \varepsilon \leq \varepsilon_{t0} \\ 1 & \varepsilon \leq \varepsilon_{tu}. \end{cases} \tag{4}$$

For the case corresponding to Fig. 3b, the tensile stress-strain curve can be divided into two segments in the post-peak region. The first part is power-law softening, valid until the stress attains the specified residual strength f_{tr}, at which the corresponding strain ε_{tr} is related to the residual strength coefficient λ ($0 < \lambda \leq 1$). ε_{tr} can be calculated as

$$\varepsilon_{tr} = \frac{\varepsilon_{t0}}{\sqrt[n-1]{\lambda}}. \tag{5}$$

The damage variable D, at any given strain, when the element is under uniaxial tension can be calculated as the following Eq. (6) under condition that $\varepsilon_{tu} < \varepsilon_{tr} \leq \varepsilon_{t0}$.

$$D = \begin{cases} 0 & \varepsilon > \varepsilon_{t0} \\ 1 - \left(\dfrac{\varepsilon_{t0}}{\varepsilon}\right)^n & \varepsilon_{tr} < \varepsilon \leq \varepsilon_{t0} \\ 1 - \left(\dfrac{\lambda\varepsilon_{t0}}{\varepsilon}\right) & \varepsilon_{tu} < \varepsilon \leq \varepsilon_{tr} \\ 1 & \varepsilon \leq \varepsilon_{tu} \end{cases} \tag{6}$$

It is possible that there is no intersection point between the power-law curve and the line denoting the residual strength if the residual strength coefficient λ is very small. In addition, if the value of ε_{tr}, which was calculated in Eq. (5), is greater than the specified ultimate strain ε_{tu}, we will not consider the influence of residual strength coefficient λ in the constitutive relation. Under this condition, Eq. (6) can be expressed as

$$D = \begin{cases} 0 & \varepsilon > \varepsilon_{t0} \\ 1 - \left(\dfrac{\varepsilon_{t0}}{\varepsilon}\right)^n & \varepsilon_{tu} < \varepsilon \leq \varepsilon_{t0} \\ 1 & \varepsilon \leq \varepsilon_{tu} \end{cases} \tag{7}$$

Additionally, we assume that the damage of mesoscopic element in multiaxial stress fields is also isotropic elastic. According to the method of extending one-dimensional constitutive laws under uniaxial tensile stress to complex tensile stress conditions, which was proposed by Mazars and Pijaudier-Cabot (1987) for a constitutive law of elastic damage, we can easily extend the constitutive law described above to a three-dimensional stress state. Under multiaxial stress states, the element still damages in tensile mode when the equivalent maximum tensile strain attains the above threshold strain ε_{t0}. Therefore, the constitutive law of element subjected to multi-axial stresses can be easily obtained by substituting the strain ϵ in Eq. (4), (6) and (7) with the equivalent principal strain $\bar{\varepsilon}$.

The equivalent principal strain $\bar{\varepsilon}$ is defined as follows:

$$\bar{\varepsilon} = -\sqrt{\langle -\varepsilon_1 \rangle^2 + \langle -\varepsilon_2 \rangle^2 + \langle -\varepsilon_3 \rangle^2}, \tag{8}$$

where ε_1, ε_2 and ε_3 are the three principal strains, and $\langle\,\rangle$ is a function defined as follows:

$$\langle x \rangle = \begin{cases} x & x \geq 0 \\ 0 & x < 0. \end{cases} \tag{9}$$

It must be emphasized that, when $D = 1$, the damaged elastic modulus is zero, which may cause the finite element analysis to halt. Therefore, a relatively small number, i.e. 10^{-5} is specified for the limit elastic modulus.

2.2.2 Constitutive Law of Mesoscopic Element Damaged in Shear Mode

The above constitutive law only considers the situation when element is damaged in tensile mode. But compressive softening also occurs when rock is subjected to compressive and shear stresses; thereafter shear damage at mesoscopic level is also

assumed to exist when the mesoscopic element is under compressive and shear stress. The Mohr-Coulomb criterion, as expressed in Eq. (10), is selected to be the second damage threshold.

$$F = \sigma_1 - \frac{1 + \sin\phi}{1 - \sin\phi}\sigma_3 \geq f_{c0}, \tag{10}$$

where σ_1 and σ_3 are the maximum and minimum principal stresses respectively. Again, compressive stresses are positive and tensile stresses are negative. As a matter of fact, the value of σ_1 and σ_3 respectively indicate the magnitude of maximum and minimum compressive stress when these two principal stresses are both compressive. Moreover, f_{c0} is the uniaxial compressive strength and ϕ is the internal friction angle of this element. We assumed that $f_{cr}/f_{c0} = f_{tr}/f_{t0} = \lambda$ is true when the element is under uniaxial compression or tension.

This kind of damage is called shear damage because damage occurs only when the stress conditions of the element meet the Mohr-Coulomb criterion. Amitrano (1999) has also utilized this criterion as an isotropic damage threshold for the damage analysis of rock.

Corresponding to the two softening schemes shown in Fig. 3, similar damage evolution laws are given in Fig. 4 when the element is under uniaxial compression and damaged in shear mode according to the Mohr-Coulomb criterion.

With regard to the constitutive law in Fig. 4a when the element is damaged in shear mode, the damage variable D can be described as follows:

$$D = \begin{cases} 0 & \varepsilon < \varepsilon_{c0} \\ 1 - \dfrac{\lambda\varepsilon_{c0}}{\varepsilon} & \varepsilon \geq \varepsilon_{c0}. \end{cases} \tag{11}$$

Corresponding to the constitutive law in Fig. 3b, the constitutive law for uniaxial compression for power-law softening can be obtained:

$$D = \begin{cases} 0 & \varepsilon < \varepsilon_{c0} \\ 1 - \left(\dfrac{\varepsilon_{c0}}{\varepsilon}\right)^n & \varepsilon_{c0} \leq \varepsilon < \varepsilon_{cr} \\ 1 - \dfrac{\lambda\varepsilon_{c0}}{\varepsilon} & \varepsilon \geq \varepsilon_{cr} \end{cases} \tag{12}$$

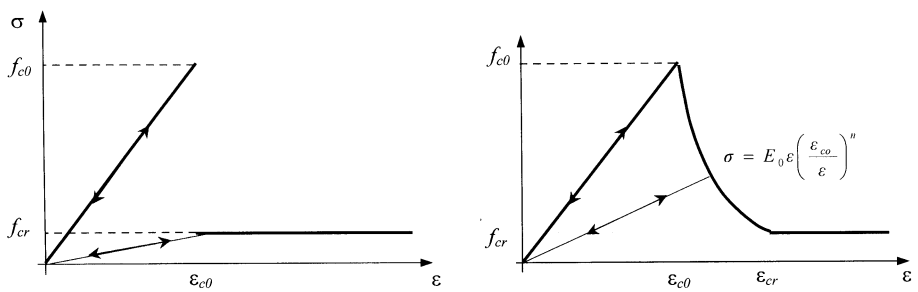

(a) Brittle with residual strength (b) Power-law softening with residual strength

Fig. 4. Elastic damage constitutive law of elements under uniaxial compressive stress (f_{c0} and f_{cr} are uniaxial compressive strength and residual corresponding strength of element, respectively)

where ε_{c0} is the strain at the peak compressive principal stress, under uniaxial compressive stress state, which can be simply calculated as

$$\varepsilon_{c0} = f_{c0}/E_0 \tag{13}$$

and ε_{cr} is calculated similarly to the ε_{tr} in Eq. (6):

$$\varepsilon_{cr} = \frac{\varepsilon_{c0}}{\sqrt[n-1]{\lambda}}. \tag{14}$$

Conditions similar to Eq. (6) are also encountered, if ε_{cr} doesn't exist, the above Eq. (12) can be expressed as:

$$D = \begin{cases} 0 & \varepsilon < \varepsilon_{c0} \\ 1 - \left(\dfrac{\varepsilon_{c0}}{\varepsilon}\right)^n & \varepsilon \geq \varepsilon_{c0}. \end{cases} \tag{15}$$

The mechanical behavior of rock in multiaxial compression is mainly characterized by a considerable increase of strength and pre-peak strain at high confinement level. When an element is under multi-axial stress state and its stress condition satisfies the Mohr-Coulomb criterion, shear damage occurs, and we must consider the effect of other principal stresses in this model during damage evolution process.

When the Mohr-Coulomb criterion is met, we can calculate the minimum principal strain (maximum compressive principal strain) ε_{c0} at the peak value of maximum principal stress (maximum compressive principal stress).

$$\varepsilon_{c0} = \frac{1}{E_0}\left[f_{c0} + \frac{1 + \sin\phi}{1 - \sin\phi}\sigma_3 - \mu(\sigma_1 + \sigma_2)\right] \tag{16}$$

In this respect, we assume that the shear damage evolution is only related to the maximum compressive principal strain ε_1. So, we use the maximum compressive principal strain ε_1 of damaged element to substitute the uniaxial compressive strain ε in Eqs. (11), (12) and (15). Thus, the former Eqs. (11), (12) and (15) can be extended to triaxial stress states for shear damage.

$$D = \begin{cases} 0 & \varepsilon_1 < \varepsilon_{c0} \\ 1 - \dfrac{\lambda\varepsilon_{c0}}{\varepsilon_1} & \varepsilon_1 \geq \varepsilon_{c0} \end{cases} \tag{17}$$

$$D = \begin{cases} 0 & \varepsilon_1 < \varepsilon_{c0} \\ 1 - \left(\dfrac{\varepsilon_{c0}}{\varepsilon_1}\right)^n & \varepsilon_{c0} < \varepsilon_1 \leq \varepsilon_{cr} \\ 1 - \dfrac{\lambda\varepsilon_{c0}}{\varepsilon_1} & \varepsilon_1 \geq \varepsilon_{cr} \end{cases} \tag{18}$$

$$D = \begin{cases} 0 & \varepsilon_1 < \varepsilon_{c0} \\ 1 - \left(\dfrac{\varepsilon_{c0}}{\varepsilon_1}\right)^n & \varepsilon_1 \geq \varepsilon_{c0}. \end{cases} \tag{19}$$

From the above expression of damage variable D, which is generally called damage evolution law in damage mechanics, together with Eq. (2), we can calcuate the damaged elastic modulus of the element at each stress or strain level. For

simplification, like other model based on elastic damage mechanics (Mazars and Pijaudier-Cabot, 1987), the Poisson's ratio of the damaged element is assumed to be constant and independent of the stress states and damage evolution process for mesoscopic element.

In this model, the mesoscopic element may gradually damage according to the above elastic damage constitutive relationship. Only elements whose ultimate tensile strain has been attained are displayed as cracks with black color in the post-processing figures. In the figure of damaged elements, all the damaged elements are denoted with different color, i.e. white and red for shear and tensile damage at current step respectively, black for all damaged elements in all the previous steps. Both tensile damage and shear damage leads to the degradation of mesoscopic elements, but tensile damage is considered to be the direct cause of crack initiation. In this respect, the initiation, propagation and interaction of multiple cracks is simply simulated. This approach to simulating cracks is similar to a smeared crack model, i.e. no special singular element is used for the finite element analysis of these mesoscopic elements, and a crack has the width of an element, which greatly simplifies the simulation of crack initiation, propagation and coalescence.

2.3 Numerical Simulation of Acoustic Emission (AE) of Rock

Monitoring acoustic emission (AE) event rates seems to be a good way to identify the initiation and propagation of cracks in rock. In quasi-brittle materials such as rock, AE is predominantly related to the release of elastic energy. Therefore, as an approximation, it is reasonable to assume that the AE counts are proportional to the number of damaged elements and that the strain energy released by damaged elements is all in the form of acoustic emissions (Tang, 1997). By this means, in this model, each AE event corresponds to damage of an element, and the AE energy release of an element is assumed to be the reduction of elastic strain energy during damage. Therefore, the AE counts are accounted by the number of damaged elements and the energy releases are calculated from the strain energies released from the damaged elements. Based on the above assumptions, the cumulative AE counts and cumulative AE energy release can be realistically simulated with the above-mentioned numerical model. Although the heterogeneous microstructure described in the numerical model is not totally consistent with that of the original rock specimens, it can reflect the stochastic characteristics to some degree due to the random distribution of material properties of rock at the mesoscopic level. More detailed descriptions about the theoretical basis of numerical simulation of AE in this model have been given elsewhere (Tang, 1997).

3. The Parameters Used in the Numerical Model

From the above-expressed constitutive relationship of mesoscopic elements, it can be seen that the constitutive law of an element depends on many parameters that include uniaxial compressive strength, Young's modulus, Poisson's ratio, internal friction angle, post-peak softening schemes, residual strength coefficient and ultimate tensile strain. The mean values of Young's modulus and uniaxial compressive strength and

their homogeneity index are the important parameters for Weibull distribution, which may directly affect the specific behavior of each element. It is generally accepted that the compressive and tensile strengths are closely related; therefore, in our model, compressive strength is assigned with a stochastic distribution and the tensile strength is obtained from a specified tensile/compressive strength ratio, which is also a material property parameter. It appears that the direct tensile/compressive ratio is 0.08 to 0.20 for rock. In the following analysis, we take the compressive/tensile strength ratio of mesoscopic element equal to 10. For convenience, the mean value of Poisson's ratio is 0.2 with a homogeneity index of 100 for its Weibull distribution, and no heterogeneity is considered for internal friction angle, which is fixed at 30° in the following calculations. The validation of these parameters can only be assessed from the results of numerical simulation.

To lay the basis of this model, the relationship between Weibull distribution parameters of mesoscopic elements and the macroscopic responses of numerical specimen should be clarified. To study the influence of these parameters on macroscopic mechanical response, specimens with homogeneity indices of 1.5 and 3.0 and 6.0, respectively, as shown in Fig. 1, are subjected to uniaxial compression by prescribing uniform longitudinal displacement at one end with the other end fixed.

Three specimens are simulated, corresponding to one given homogeneous index. At the same time, the influence of ultimate tensile strain, residual strength coefficient, as well as the softening schemes of constitutive law in the post-peak region is included in the analysis. The following schemes of elements at the post-peak region are included in the analysis: brittle with residual strength (called "brittle" in Table 1), and two power laws with different parameter $n = 2$, 5. The values of η and λ are based on general knowledge from the macroscopic stress-strain characteristics of rock specimens carried out in the laboratory. The values of all these parameters are listed in Table 1.

In the previous paper (Zhu et al., 2002), the effect of these parameters on macroscopic stress-strain response has been presented in order to study the fracture behavior of concrete, and some results are given as follows.

3.1 Effect of Homogeneity Index and Constitutive Parameters

Typical stress-strain curves of numerical specimens with different ultimate strain coefficients and residual strength coefficients, for homogeneity index 1.5, are given in Fig. 5. The stress-strain curves with three softening schemes of mesoscopic constitutive law are drawn in each figure. Given this homogeneity index, the stress-strain

Table 1. Parameters of the constitutive law for studying the model

Homogeneity index (m)	Ultimate tensile strain coefficient (η)	Residual strength coefficient (λ)	Softening schemes (n)
1.5	2.0	0.00001	2
3.0	3.0	0.01	5
6.0	5.0	0.1	"brittle"

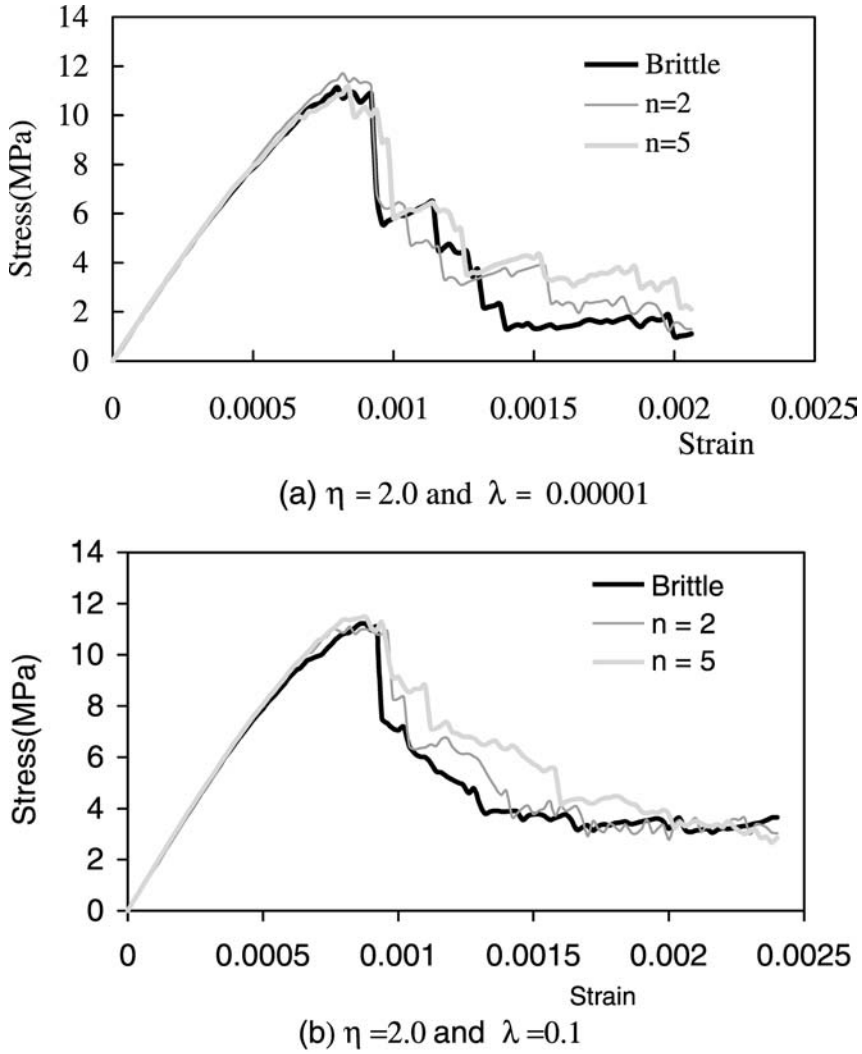

Fig. 5. Stress-strain curves of numerical specimens when homogeneity index $m = 1.5$ (numerical results)

curves show distinct non-linearity in the pre-peak region. The specimen loses its loading capacity gradually, and the failure is stable. It is seen that the three different softening schemes yield roughly the same macroscopic stress-strain curves although some scatter exists in the results.

Comparing Fig. 5a and Fig. 5b, we can find that not only the peak stresses but also the initial Young's moduli are approximately the same. However some difference exists at the post-peak region of these stress-strain curves. It is also found that the increase of ultimate tensile strain coefficient may enhance the peak stress although this tendency is not very strong even if the ultimate tensile strain coefficient is very large. Moreover, an increase of ultimate tensile strain coefficient does not lead to the

enhancement of ductility of stress-strain of numerical specimens under this kind of homogeneity index, i.e. $m = 1.5$. Therefore, it can be concluded that the parameters, such as softening schemes of constitutive law, ultimate tensile strain coefficient, as well as residual strength coefficient, have very little effect on the stress-strain response of numerical specimens when the homogeneity index is 1.5.

In Fig. 6, we give the stress-strain curves corresponding to the same conditions shown in Fig. 5, when the homogeneity index $m = 3$. Because of the enhancement of homogeneity index, the Young's modulus and strength are more homogeneous (as shown in Fig. 1) compared to those of Fig. 5, and thus the macroscopic strengths and Young's moduli of these numerical specimens are increased. The stress-strain curves

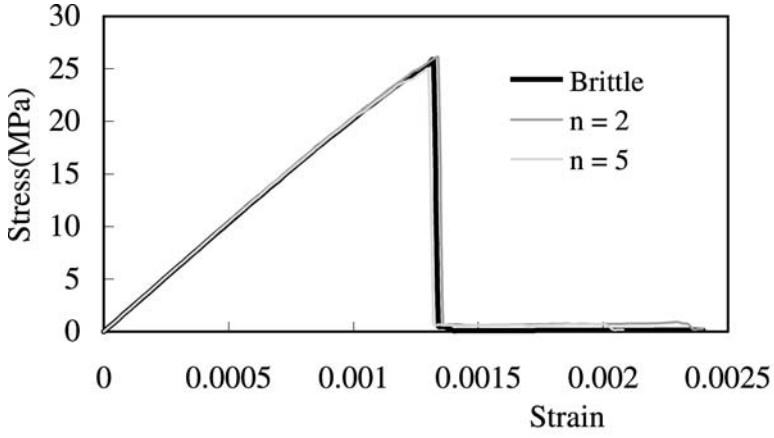

(a) $\eta = 2.0$ and $\lambda = 0.00001$

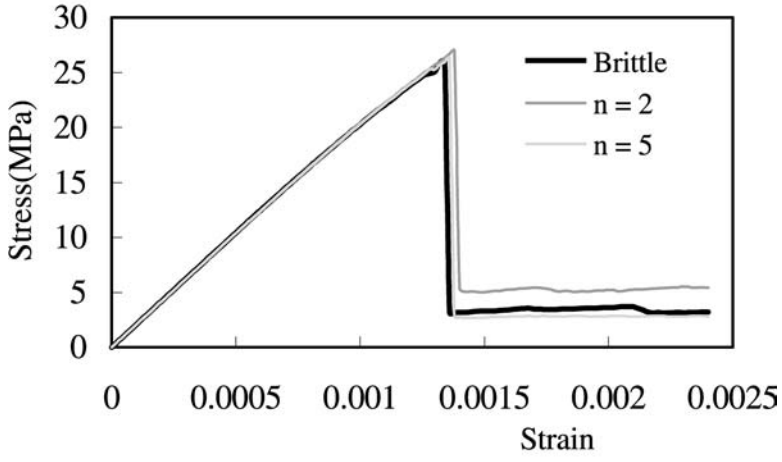

(b) $\eta = 2.0$ and $\lambda = 0.1$

Fig. 6. Stress-strain curves of numerical specimens when homogeneity index $m = 3.0$ (numerical results)

of these numerical specimens are basically linear in the pre-peak region, and lose most of their load-carrying capacity abruptly when many elements damage at the same time and release a large amount of strain energy. Therefore, these specimens fail in an unstable manner when macrocracks suddenly appear, producing stress-strain curves that are very brittle. From the above results, we can conclude that the heterogeneity index in this model not only controls the strength and ductility but also affects the stability of crack propagation in the materials.

The above numerical results indicate that in this micromechanical model the non-linear material behavior arises from its heterogeneous material properties, and does not depend on the post-peak softening schemes of the constitutive law. This situation is quite different from a conventional analysis, using various constitutive relationships and homogeneous properties, because in that case the non-linearity of materials arises from the complex nonlinear constitutive model. Therefore, it can be deduced that the macroscopic nonlinearity of the proposed model comes from its internal heterogeneous structure, and the more heterogeneous the material properties are, the stronger is the non-linearity in the stress-strain response. Tang (1997) proposed that heterogeneity is the source of non-linearity with regard to brittle materials such as rock and how the global non-linear behavior observed in these brittle materials can be reproduced with brittle-elastic elements if heterogeneity is included. Therefore, a very simple elastic-brittle constitutive law with residual strength, as proposed in this paper, is sufficient to describe stress-strain characteristics at the mesoscopic level (Tang, 1997).

As mentioned above, the mean uniaxial compressive strength of elements of the entire numerical specimen is 100 MPa, but calculated uniaxial compressive strengths are considerably lower than this value, namely 11.5, 26.1, and 42.9 MPa, when the homogeneity indices are 1.5, 3.0 and 6.0, respectively. That is to say, the macroscopic strength is usually far lower than the average value of element parameters, because the strength of a specimen is mainly governed by the weakest elements. As the homogeneity index increases, material properties become more homogeneous and approach that of the homogeneous body; the Young's modulus and strength of every element approach their mean value given in the Weibull distribution (as shown in Fig. 7). In Fig. 7 the values of calculated elastic modulus and strength of the numerical specimens are all normalized with respect to their mean values of Weibull distribution parameter u_0. We find that the homogeneity index m has much more influence on the macroscopic strength than that on elastic modulus. In Fig. 7b, the fitted equations for normalized strength and elastic modulus when homogeneity indexes m smaller than 10.0 are also presented. Only when all the mesoscopic elements in the specimen have the same mechanical parameters would all elements in the numerical specimen damage simultaneously when subjected to uniaxial compression, and the stress-strain curve of numerical specimen would exactly coincide with the constitutive law of elements (as shown in Fig. 8). This also proves that the finite element analysis used in RFPA is correct.

3.2 Effect of Spatial Distribution of Material Properties

Even with the same distribution parameters for each specimen, the spatial distribution of properties of elements may be stochastically different. In order to investigate this

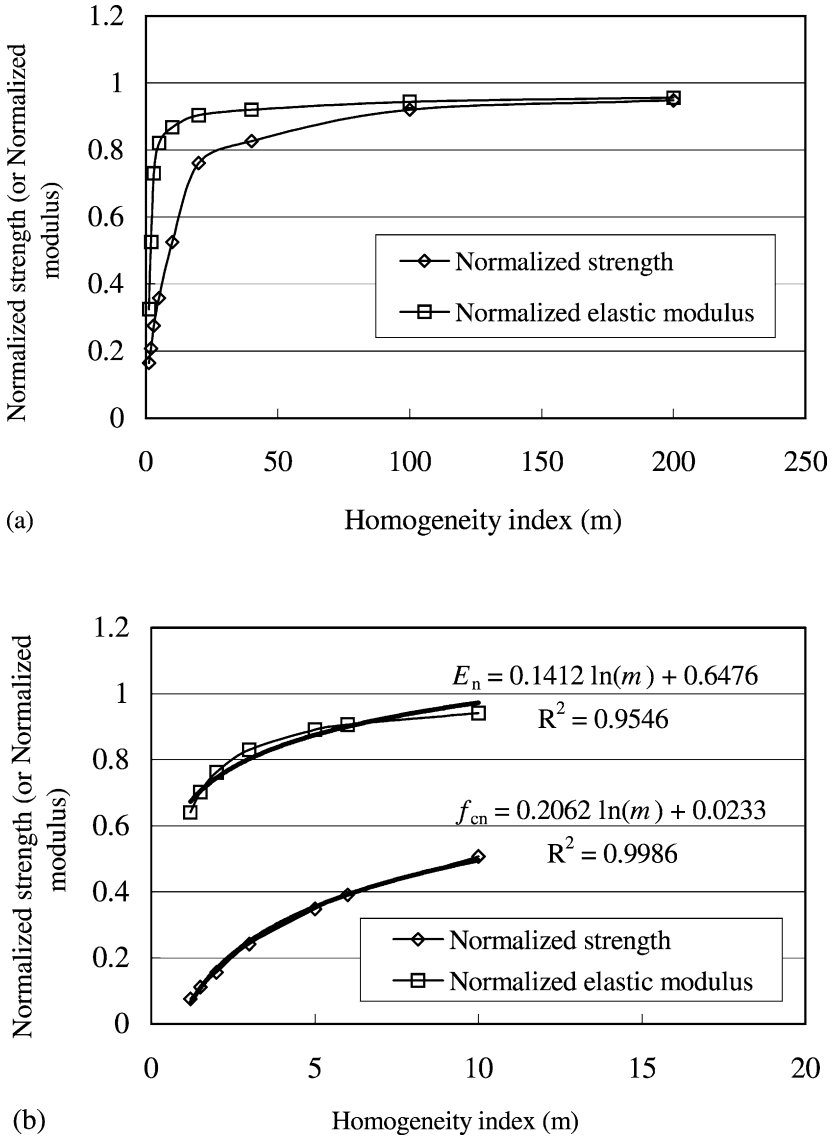

Fig. 7. Influence of the homogeneity index on the macroscopic elastic modulus and strength (numerical results). **a** Curves of normalized strength and elastic modulus when $1.2 \leq m \leq 200$, **b** Fitted equations for normalized strength and elastic modulus when $1.2 \leq m \leq 10$

randomness due to the spatial distribution of elements, three numerical specimens whose material properties are specified randomly according to the same Weibull distribution parameters are studied. The numerical results show that macroscopic mechanical responses, such as initial elastic modulus and uniaxial compressive strength, are very close to each other (see Fig. 9) although some scatter exists in their post-peak zone of the stress-strain curves, especially when the heterogeneity

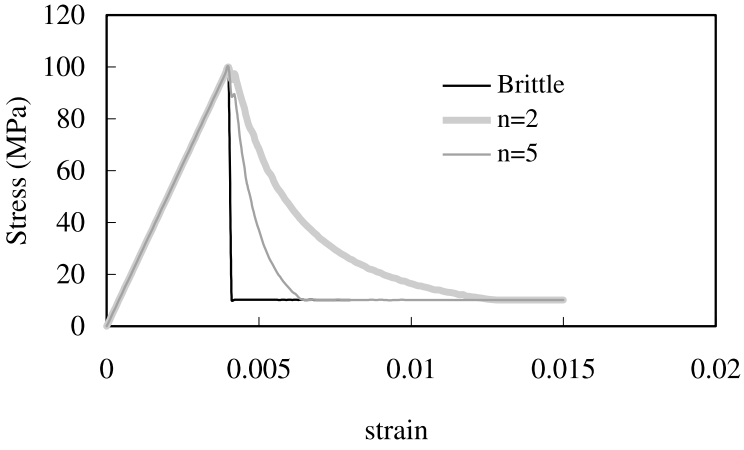

Fig. 8. Stress-strain curves of homogeneous specimens for different schemes of constitutive law (numerical results)

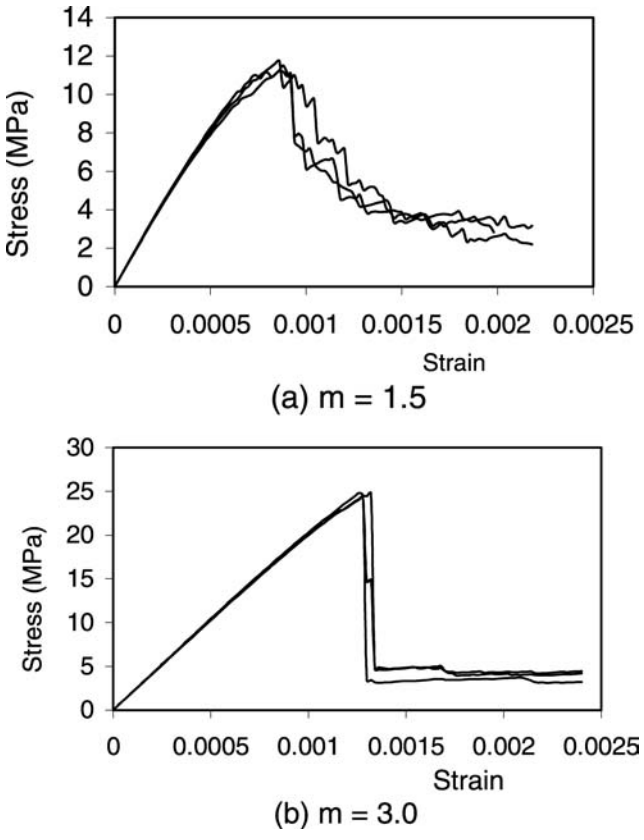

Fig. 9. Stress-strain curves of three specimens with same homogeneity index (numerical results)

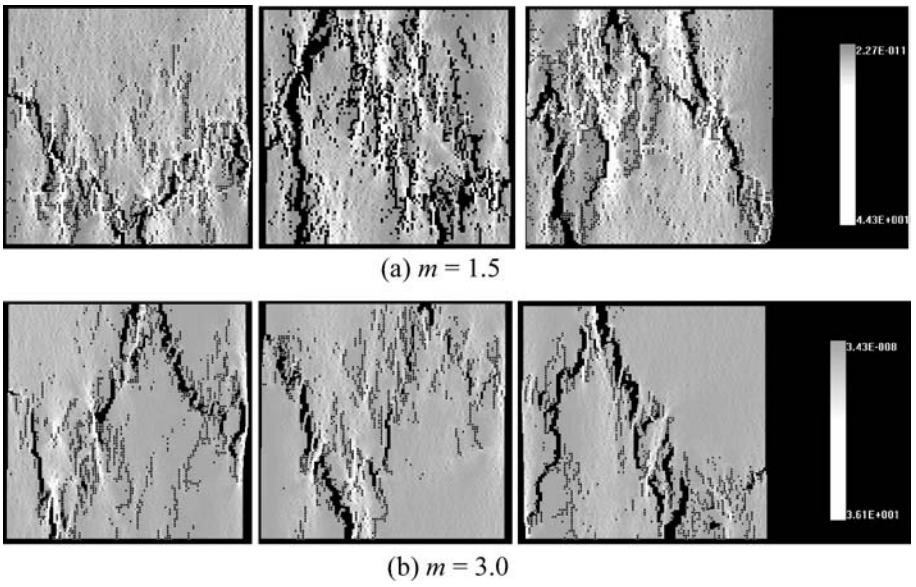

Fig. 10. Failure patterns of three specimens with same Weibull distribution (numerical results)

of specimen is larger, for example, $m = 1.5$ (see Fig. 9). Owing to the randomness of spatial distribution of material properties, the cracking patterns of different numerical specimens may be quite different, although they all appear to undergo splitting failure due to tensile cracking. But we think that this difference actually reflects the influence of spatially stochastic distribution of material properties, showing that the spatial arrangement of elements with different mechanical properties heavily influences which element attains its strength at first, leading to different cracking patterns (as shown in Fig. 10). In Fig. 10, the grey degree in the figure denotes the magnitude of strength of elements. The elements with lighter color have relative high maximum shear stress. The totally damaged elements are displayed as black. Under this kind of loading conditions, the specimens all begin from the tensile failure of separate elements, then the damaged elements coalesce with others, until, eventually, the macroscopic failure band is formed. With specimens with high homogeneity index, the macroscopic failure bands are more concentrated compared to specimens with low homogeneity index. By contrast, the more heterogeneous specimens has higher residual stress after failure (as shown in Fig. 10).

3.3 Effect of Number of Elements

Given numerical specimens with a fixed size of 100 mm $\times$ 100 mm, some differences may exist if we simulate them with 50×50 or 150×150 elements, compared to that with 100×100 elements. Figure 11a gives the stress-strain curves of 100 mm $\times$ 100 mm specimens when they were simulated respectively with 50×50, 75×75, 100×100 and 150×150 elements, with identical Weibull distribution parameters. It is found that the increase of number of elements leads to a significant decrease

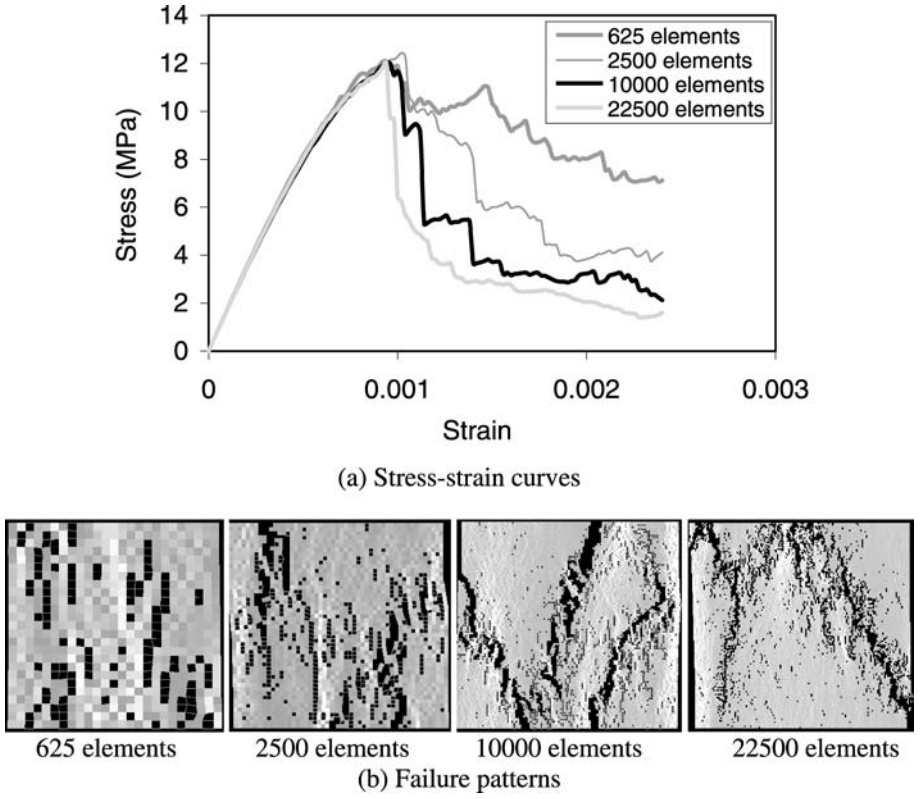

Fig. 11. Effect of number of elements on stress-strain curves and failure patterns of numerical specimens (numerical results)

of ductility, which can be observed from the macroscopic stress-strain curves. However the number of elements has a minor influence on the macroscopic strength and failure patterns of the numerical specimens (as shown in Fig. 11b).

In order to indicate how the number of elements affects the brittleness of numerical specimens, the quantification of the brittleness is necessary. As shown in Fig. 12, the stress-strain curve of rock can be divided into two segments, i.e. pre-peak segment and post-peak segment. A brittleness index B is defined as the ratio of area I and II, in Fig. 12, expressed by the following equation

$$B = \frac{\int_0^{\varepsilon_0} \sigma\varepsilon \, d\varepsilon}{\int_{\varepsilon_0}^{2\varepsilon_0} \sigma\varepsilon \, d\varepsilon} \tag{20}$$

where ε_0 is the strain at the peak stress. This definition is applicable to the stress-strain curves of uniaxial tensile and compressive stress states.

The relationships between brittleness index B and number of elements can be obtained when the homogeneity index is 1.5 and 3.0 respectively, as shown in Fig. 13. The solid lines are the linear fit from the numerical results. It can be seen that an almost

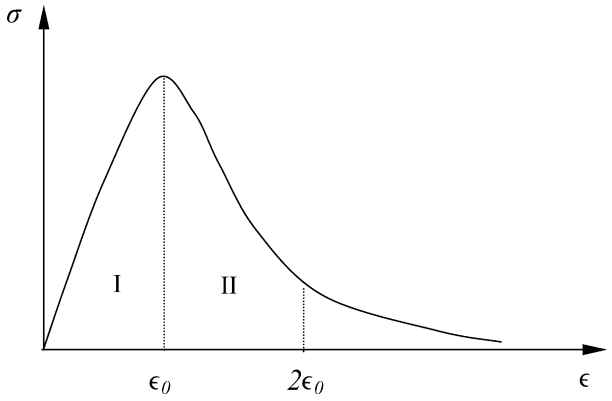

Fig. 12. Derivations of brittleness index B

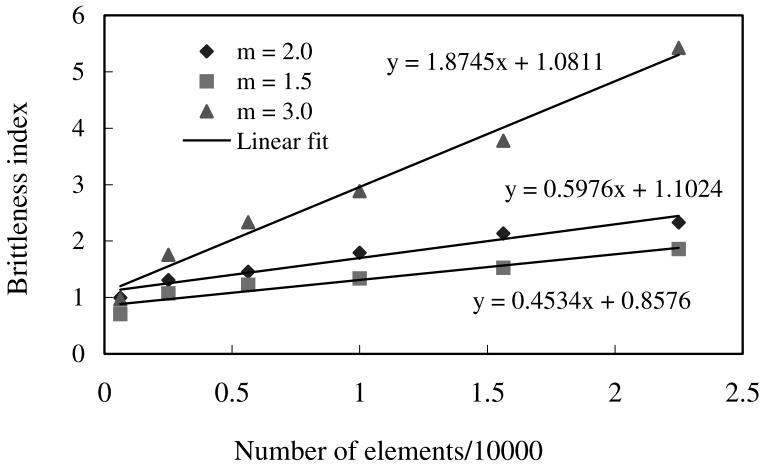

Fig. 13. Relationship between the number of elements and brittleness index of stress-strain curve (numerical results)

linear relationship exists between the number of elements and brittleness index B for a given homogeneity index (Fig. 13). The number of elements comprising a specimen has little effect on the macroscopic elastic modulus and strength of the specimens.

In the RFPA the material properties of the given number of elements are randomly specified according to Weibull distribution. According to the opinions of some researchers on the size of mesoscopic level (Aliabadi, 1999), it is generally accepted that a size of $1\,\text{mm} \times 1\,\text{mm}$ elements is acceptable in the numerical simulation of standard rock specimens for laboratory tests. In order that the brittle index of stress-strain characteristics provided by numerical simulation can reflect true material properties, we should decrease the homogeneity index if we must increase the size of element due to the limit of computer capacity. For example, when we simulate a specimen of $100\,\text{mm} \times 100\,\text{mm}$ with 100×100 elements under the homogeneity

index of 1.5, the obtained brittleness index is 1.35. If we simulate this specimen with 50×50 elements, the selected homogeneity index should be between 2.0 and 3.0 in order to reflect the same brittleness. Based on the given relationship between number of elements and brittleness index under a certain homogeneity index, we can simulate the stress-strain characteristics of rock with fewer elements, which can significantly increase the efficiency of the model.

Therefore, when we carry out numerical simulations with this model, the brittleness index of this rock should be based on uniaxial compressive laboratory test results. Then the number of elements, as well as the brittleness index, is selected according to the capacity of computer and the brittleness index. The average of the uniaxial compressive strength as well as the elastic modulus of mesoscopic elements should be determined according to the relationship of mechanical properties between the mesoscopic elements and their assembled macroscopic response as given in Fig. 7.

The aforementioned discussions about the parameters used in this model are based on numerical results of numerical specimens in uniaxial compression. How the Weibull distribution parameters, such as mean values of material properties and homogeneity index, constitutive parameters that include residual strength coefficient λ, ultimate strain coefficient η, and the number of elements affect the numerical results, is discussed in length. In order to simplify the analysis, other constitutive parameters such as internal cohesive angle ϕ, tensile/compressive strength ratio are fixed throughout all the calculations. Our extensive study indicates that the above results are universally applicable to conditions when the numerical specimen is under uniaxial tension. In addition, the compressive/tensile strength ratio can also be obtained after simulating both a uniaxial compression test and a uniaxial tension test on a numerical specimen. It is observed that the compressive/tensile strength ratio obtained from numerical simulation is between 8 and 12, which depends on the given compressive/tensile strength ratio of all mesoscopic elements.

4. Implementation of Micromechanical Model

Numerical simulation is considered to be the third tool for scientific research. It can give an approximate behavior of material and structures at best using reasonable and powerful numerical models. Basically, numerical simulation of fracture process in rock must be carried out at mesoscopic level. Laboratory test of rock material, which is considered to be at macroscopic level, can be simulated with RFPA model at mesoscopic level. Information from the mesoscopic structure of the material must be incorporated into the model. The process of numerical simulation using the RFPA model can be divided into three steps.

The first step involves model setup and generation of material heterogeneity, which consists of the selection of Weibull distribution parameters, constitutive parameters of mesoscopic elements, and number of elements to represent the rock numerically. Input data for the analysis include the strength and stiffness of the constituents of the materials. Such properties must be determined from other, lower-level, material properties experiments. However, few real experiments are usually done at mesoscopic level for materials like rock. The selection of parameters used in the model is generally based

on the principle that the numerical specimen produced with RFPA matches some basic mechanical properties such as Young's modulus, uniaxial compressive strength, uniaxial tensile strength and brittleness index of real rock. More elements are necessary in order to describe the heterogeneity of material at mesoscopic level, but due to the limit of computer capacity, sometimes it is necessary to regulate the homogeneity index to reflect the brittleness of the real material. Weibull distribution parameters is specified based on the relationship between material properties of mesoscopic elements and macroscopic response, as given in Fig. 7.

The second step in the numerical simulation is to specify the boundary conditions and loading condition. In order to obtain the complete stress-strain curve as well as the fracture process, a displacement-controlled loading scheme is usually adopted.

In the third step, the finite element analysis based on the given damage threshold and constitutive law of meso-level elements is carried out. The specified displacement applied at one end of specimen is increased step by step, the elements in the specimen are damaged and their mechanical parameters degrade according to the elastic damage constitutive law. If some elements damage at a certain step, recalculation at current boundary and loading condition must be implemented to achieve the stress redistribution in the specimen until no new damage occurs. Then the external load (or displacement) is increased and the program goes into the analysis of next step.

A variety of post-processing results can be obtained, such as distribution of stress and displacement, load-displacement response and cracking pattern during the complete failure process of numerical specimen.

From the preceding description, it appears that this model can be easily used for numerical simulation of three-dimensional problems because the constitutive law is based on the triaxial stress states, and since the FEM program for stress analysis is easy to extend for three-dimensional stress analysis. More elements must be included in order to reflect the mesoscopic heterogeneity when carrying out the three-dimensional failure analysis of material; at present we don't have sufficient computer power to carry out this kind of numerical simulation.

5. Numerical Simulation of Rock Fracture

5.1 Numerical Model of Rock Specimen

The rock is assumed to be a heterogeneous material, and its mechanical properties are considered to conform to the Weibull distribution. For simplification, it is assumed that the elastic modulus and strength have the same homogeneity index. The rock specimen is simulated with 100×100 mesoscopic elements. The mechanical parameters of each phase are listed in Table 2.

Table 2. Material properties for rock specimen

Parameters	Value
Homogeneity index (m)	3.0
Mean compressive strength (σ_0)	120 (MPa)
Mean elastic modulus (E_0)	22000 (MPa)

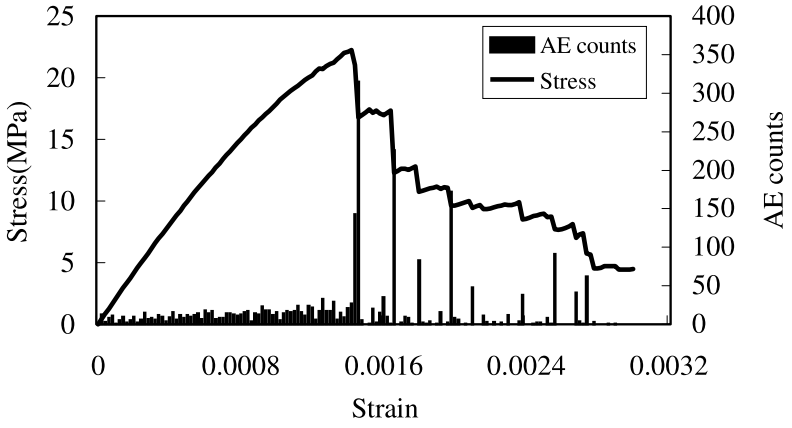

Fig. 14. Stress-strain curve and AE counts of rock under uniaxial compression (numerical results)

The complete fracture characteristics of a numerical specimen under uniaxial or biaxial loading may be investigated only in a stable displacement-controlled test. The load is applied in the vertical direction through displacement control at one end, while the other end is prevented from vertical movement. Similar boundary conditions are also designated in the horizontal direction for the biaxial loading condition.

5.2 Numerical Simulation of Rock Under Uniaxial Loading

The stress-strain curves as well as the AE counts during the fracture process of this numerical rock specimen under uniaxial compression are shown in Fig. 14. The stress-strain curve shows an ascending branch, a peak and a descending branch or softening branch. The strength and elastic modulus of this numerical specimen of rock is 22.3 MPa and 21.0 GPa respectively. It can be clearly seen that there are damaged elements when a very small load is applied. But these damaged elements release much less energy, therefore the curve is nearly linear up to approximately 60% of the maximum load. Localization of deformations may appear due to cracking caused by these damaged elements. After reaching the peak load, the load-carrying capacity of rock drops considerably, followed by a long tail until fracture of the specimen.

In Fig. 15, the AE distribution, cracking patterns and maximum shear stress distribution are presented. In the figure of AE distribution (as shown in Fig. 15a), all the damaged elements are denoted with different color, i.e. white and dark grey for elements damaged in shear and tensile mode at current step respectively, and black for damaged elements in all the previous steps. Fig. 15b denotes the magnitude of elastic modulus of mesoscopic elements. The damage of elements causes degradation of their elastic modulus and totally damaged elements will be displayed as black color; thus, such a display illustrates the cracking patterns of the rock specimen during the complete fracture process. As shown in Fig. 15c, the brightness in the maximum shear stress figures indicates the magnitude of maximum shear stress.

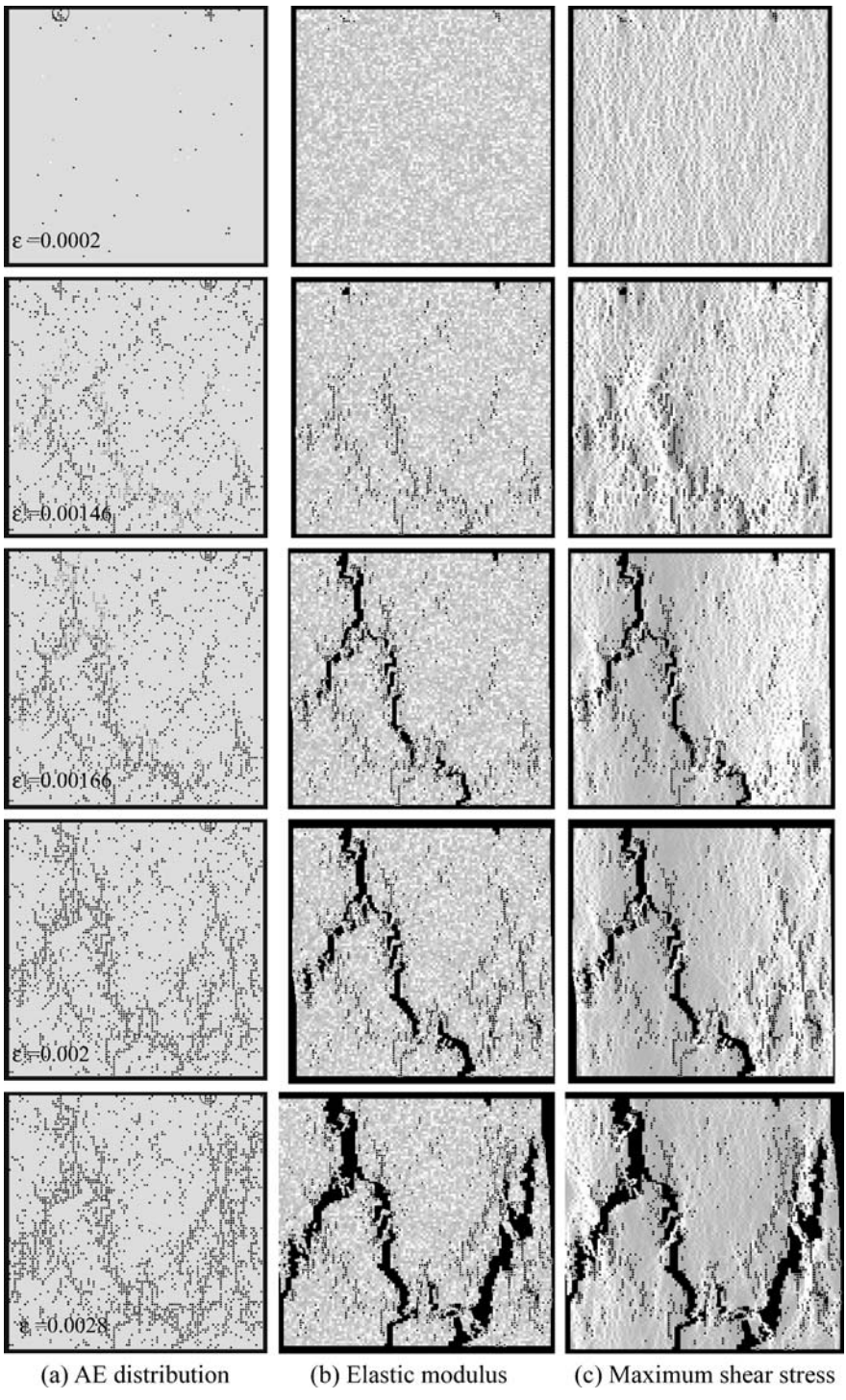

Fig. 15. Failure process of rock specimen under uniaxial compression (numerical results)

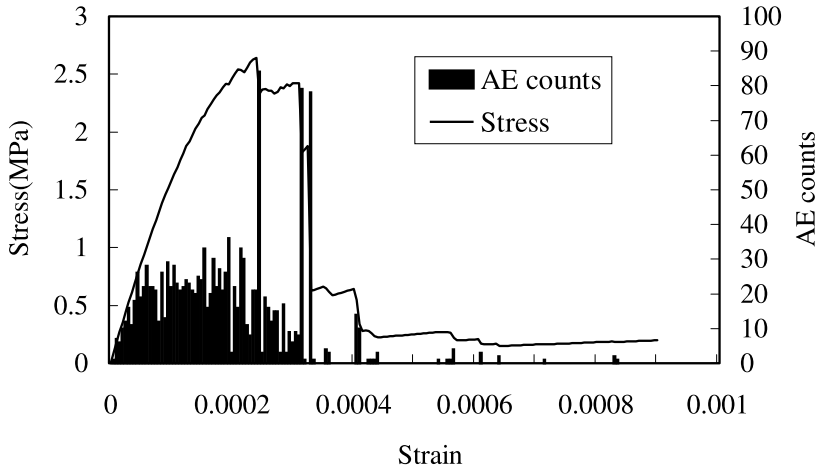

Fig. 16. Stress-strain curve and AE counts of rock under uniaxial tension (numerical results)

From Fig. 15a, it can be seen that crack propagation is dominantly caused by tensile damage. It can be seen that the fracture of rock in uniaxial compression is essentially caused by the tensile cracking of mesoscopic elements. Macroscopic fracture bands are formed at an angle of 20 to 30 degrees inclined to the direction of the applied load. The failure process and the final pattern are quite similar to experimental results on rock.

When the numerical specimen is subjected to uniaxial tension, a stress-strain curve as shown in Fig. 16 is obtained. Many of the phenomena described before for uniaxial compression also apply to this stress state. Under this stress state, the mesoscopic elements would be totally damaged in tensile mode. Comparing the AE counts with those obtained under uniaxial compression, much more elements are damaged in tensile mode at the beginning. Along with the increase of load, the curve becomes nonlinear. Due to the heterogeneity, the specimen also loses its load-carrying capacity gradually. The macrocracks are predominantly orthogonal to the direction of tensile loading. The failure pattern is shown in Fig. 17. These cracking patterns obtained in the numerical simulation are very similar to those obtained experimentally. The tensile strength of this specimen is 2.26 MPa, thus the compressive/tensile strength ratio is $22.3/2.6 = 8.5$, which is within the range of experimental values for rock. From Fig. 17, the initiation and propagation of microcracks, stress concentration at the crack tip, as well as the stress redistribution due to crack propagation and localization of deformation, is evident.

5.3 Numerical Simulation of Rock Under Biaxial Loading

The question of the behavior of rock under biaxial compression is of both fundamental and practical significance. Many experiments on rock specimen subjected to biaxial compression had been done in the past (Brown, 1976; Maso and Lerau, 1980; Kim and Lade, 1984; Amadei, 1988). Here we used the numerical specimen, which has been

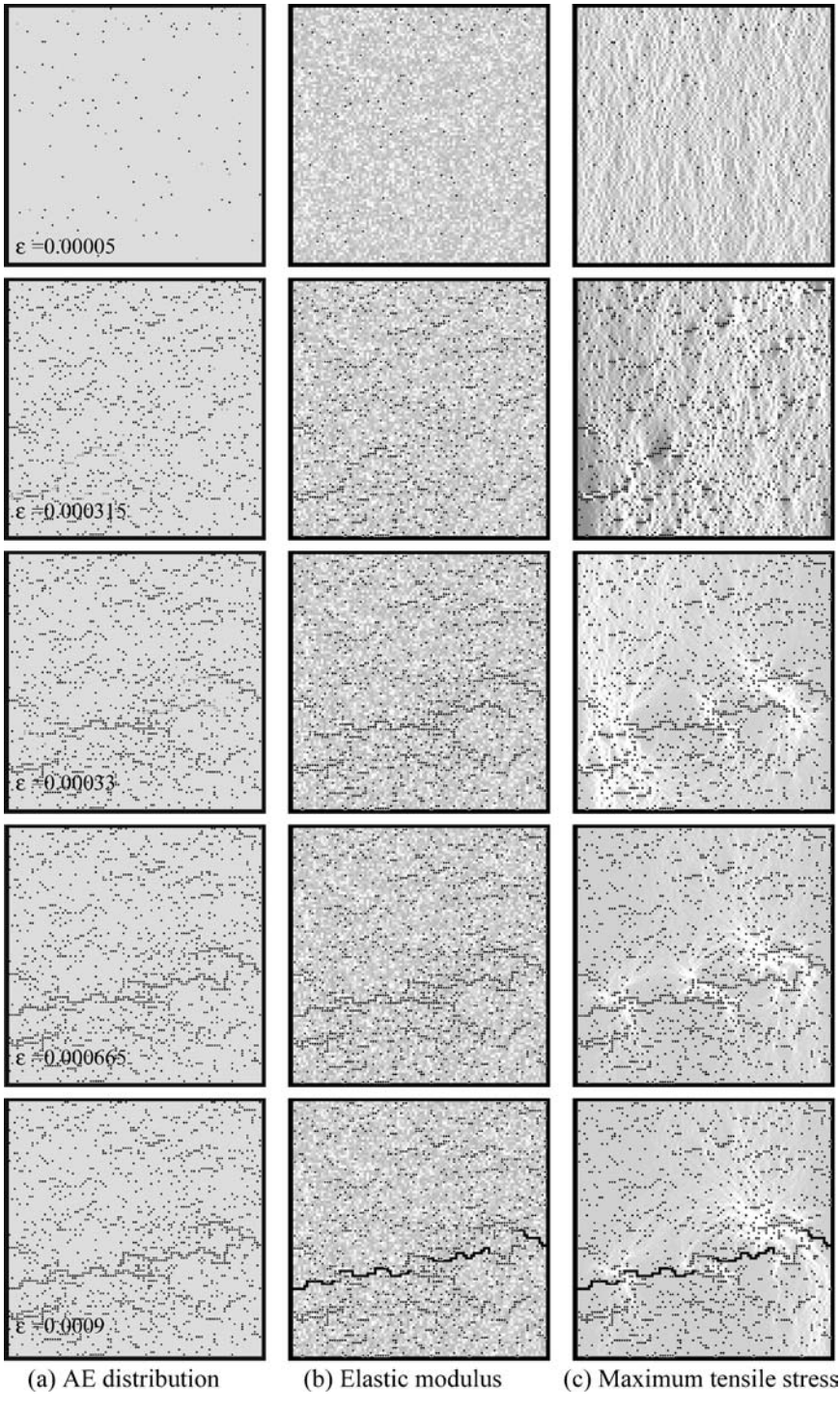

Fig. 17. Failure process of rock specimen under uniaxial tension (numerical results)

previously subjected to uniaxial loading and whose macroscopic response has been determined, to study its failure characteristics under biaxial loading. The two principal stresses, i.e. σ_x and σ_y are applied in horizontal and vertical direction on the numerical specimen. The monotonic proportional biaxial loading is gradually applied in two vertical directions with load control. The numerical simulations of this rock specimen, which are considered as plane stress states, are carried out in the biaxial stress regime with $\sigma_x/\sigma_y = +0.5/+1$, $+0.2/+1$, $+1/+1$, $-1/+10$, $-1/+5$, and $-1/-1$. These 6 stress ratios cover the entire range of compression-compression, compression-tension, and tension-tension loading conditions. In combination with the numerical results of a numerical specimen subjected to uniaxial compression and tension, the biaxial strength envelopes of this numerical rock specimen can be obtained numerically, and are shown in Fig. 18. All the numerical results are normalized to the uniaxial compressive strength. It is found that the numerical results show good agreement with experimental results. It can be seen that the strength envelopes from numerical simulation compare favorably with those of experimental results of rock specimen when a brush platen was used between specimen and test machine (Brown, 1976).

Note that the existence of a descending branch of the stress-strain curve as well as the complete failure process can't be obtained under this load-controlled loading scheme. With a displacement-controlled loading scheme, the descending portions of stress-

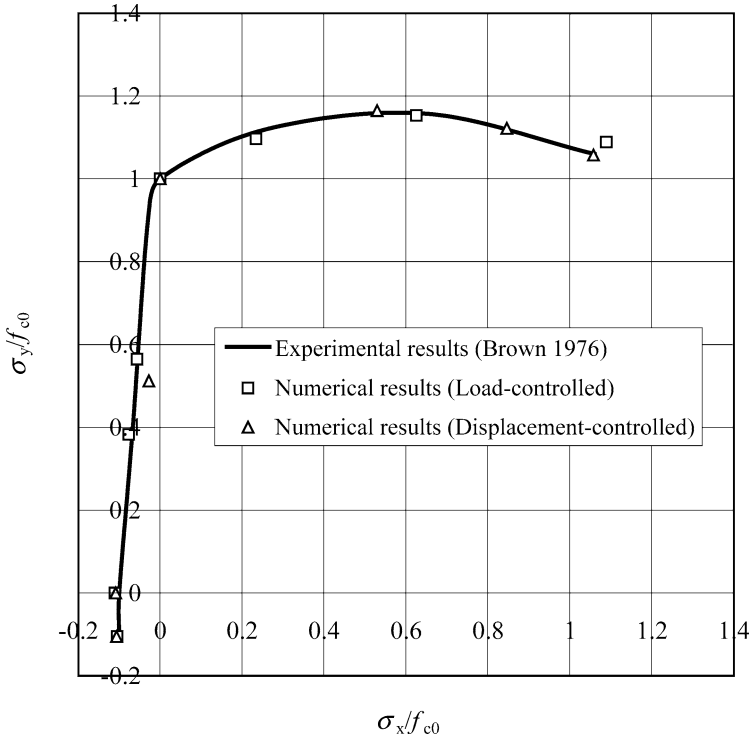

Fig. 18. Biaxial strength envelopes of rock (experimental and numerical results)

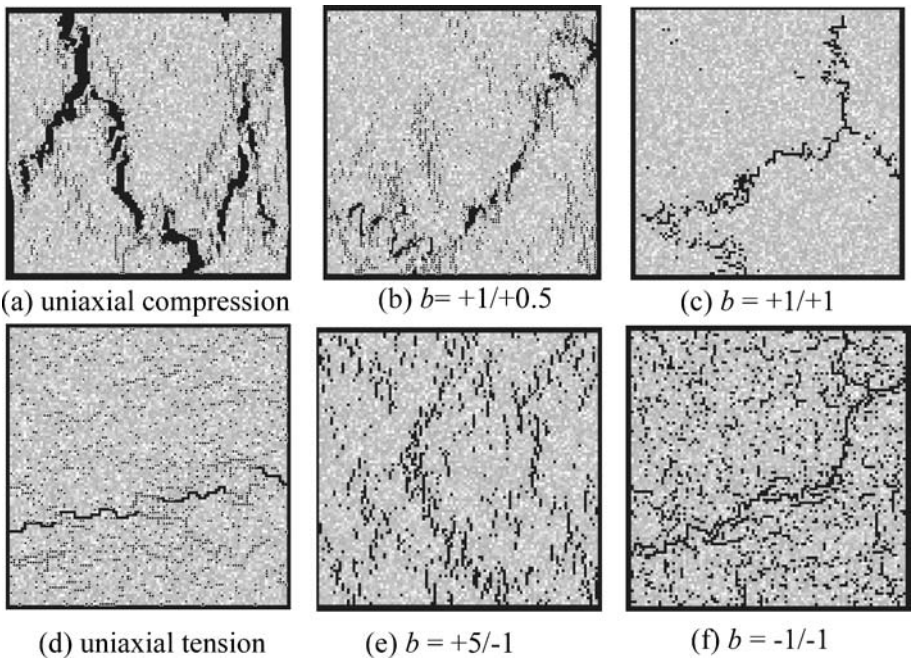

Fig. 19. Failure patterns of rock specimen under uniaxial or biaxial loading (numerical results)

strain curves, crack propagation process, localization of deformation as well as the cracking patterns during the complete fracture process of this numerical specimen could be simulated. The displacements applied in two directions are indicated with u_1 and u_2, respectively. Here b represents the ratio of u_x/u_y, where $b = +0.5/+1$, $+0.2/+1$, $+1/+1$, $-0.1/+1$, $-0.2/+1$, and $-1/-1$. The typical failure patterns of this specimen under different combinations of biaxial loading conditions (including uniaxial compression and tension) are shown in Fig. 19. Under this kind of loading scheme, the stresses in vertical and horizontal direction when specimen fails is also obtained, and drawn in Fig. 19. Of course, sometimes stresses in the two directions attain their peak values at the different loading levels, due to the specimen heterogeneity. That is to say, a quite different stress path is activated on this numerical specimen of rock under a displacement-controlled loading scheme. We find that the strength values obtained from the displacement-controlled loading method are also in agreement with the experimental results. From the above numerical simulation, it is concluded that the loading path has a small effect on the strength envelope of rock under biaxial loading. This conclusion was also obtained for concrete, as reported by Kupfer and Gerstle (1973).

It can be seen that the transverse tensile strains induced in numerical specimens under uniaxial compression are greatly decreased due to application of compression load in the lateral direction. In addition, this lateral load also reduces the tensile stress concentration that is found when the rock specimen is under uniaxial compression. Consequently, application of a lateral load improves the load-carrying capacity of rock specimens. On the other hand, lateral load on the specimen causes some additional

tensile strain in the third direction, which leads to failure under biaxial compression. This can explain why the enhancement of biaxial compressive strength of rock is somewhat limited when compared to its uniaxial compressive strength. Under biaxial compressive loading, there are generally one or two inclined fault planes as shown in Fig. 19.

Because the numerical simulation is carried out as a plane stress problem, we cannot simulate the failure phenomena orthogonal to the loading plane. Therefore, the failure mechanism simulated under these conditions derivates from reality. However, the complex stress distribution in the specimen under this stress state can be numerically simulated (as shown in Fig. 19), and the failure patterns in the loading plane resemble somewhat those of experimental results (Brown, 1976; Maso and Lerau, 1980). The actual fracture mechanism of concrete subject to biaxial compression can only be simulated by using three-dimensional numerical simulation.

Under combined compression and tension, cracks parallel to the applied compressive stress are easier to form compared with those under uniaxial compression, because the lateral tensile stress promotes the initiation and propagation of splitting cracks. One or more continuous cracks normal to the principal tensile stress are usually formed, and show similar cracking characteristics to uniaxial compression tests. The failure patterns of rock under compression-tension from numerical simulation in this paper are also similar to the corresponding experimental results (Brown, 1976; Amadei, 1988).

Under biaxial tension, failure occurs by the formation of a single crack perpendicular to the direction of the maximum tensile stress. For equal biaxial tension, there is no preferred direction for the fracture surface, it can be found that a zigzag crack crosses over the whole specimen (also see Fig. 19) concurrently in two loading directions.

6. Conclusions

In this paper, the constitutive law used in RFPA is described with elastic damage mechanics and some parametric analyses are carried out to validate the RFPA model. The failure process of rock subjected to uniaxial or biaxial loading is simulated with the RFPA model and compares well with experimental results. The following conclusions can be drawn:

1) The heterogeneity of material is based on the assumption that mechanical properties of mesoscopic elements conform to the Weibull distribution.
2) The influences of the parameters used in the constitutive law on the macroscopic response of numerical specimens are discussed in detail. The very simple elastic-brittle constitutive law is sufficient to simulate the non-linearity of rock when the heterogeneity of material properties is incorporated in the numerical model.
3) The numerical model predicts favorably the strength envelopes of rock under different combinations of biaxial loading conditions. Further, the numerical results also indicate that the biaxial strength envelope of rock is independent of the loading path.
4) The mesoscopic numerical model used in this paper is capable of modelling the crack propagation process and other fracture characteristics of rock subjected to uniaxial and biaxial loading, which show good agreement with those observed in the experiments. As a further validation of this model, the relationship between

mesoscopic structure (such as pore, microcrack in rock) and Weibull distribution parameters of numerical specimen should be tested in order to make the numerical specimen reflect the microstructures of rock properly.

Acknowledgements

This work presented in this reprot is supported by the National Natural Science Foundation (Grant No. 50174013, 50134040 and 50204003) of P.R.China. The authors are grateful for this support.

References

Aliabadi, M. H. (1999): Fracture of rock. Computational Mechanics Publications, WITPRESS Boston, Southampton.

Amadei, B. (1988): Strength of a regularly jointed rock mass under biaxial and axisymmetric loading conditions. Int. J. Rock Mech. Min. Sci. Geomech. Abstr. 25(1), 3–13.

Amitrano, D. (1999): From diffuse to localized damage through elastic interaction. Geophys. Res. Lett. 26(14), 2109–2112.

Blair, S. C., Cook, N. G. W. (1998): Analysis of compressive fracture in rock statistical techniques: Part I: A non-linear rule-based model. Int. J. Rock Mech. Min. Sci. 35, 837–848.

Bobet, A., Einstein, H. H. (1998): Fracture coalescence in rock-type materials under uniaxial and biaxial compression. Int. J. Rock Mech. Min. Sci. 35(7), 863–888.

Brown, E. T. (1976): Fracture of rock under uniform biaxial compression. In: Proc., 3rd Congress of International Society for Rock Mechanics. Denver, CO, USA, 111–117.

Carpinteri, A., Chinaia, B., Nemati, K. M. (1997): Complex fracture energy dissipation in concrete under different loading conditions. Mech. Mater. 26(2), 93–108.

Chinaia, B., Vervuurt, A., Van Mier, J. G. M. (1997): Lattice model evaluation of progress failure in disordered particle composites. Engng. Fract. Mech. 57(2/3), 301–318.

Chudnowski, A., Kunin, B. (1987): A probabilistic model of brittle crack formation. J. Appl. Phys. 62, 4124–4133.

Cundall, P. A. (1988): Formation of a three-dimensional distinct element model, Part I. A scheme to detect and represent contacts in a system composed of many polyhedral blocks. Int. J. Rock Mech. Min. Sci. 25, 107–116.

Eberhardt, E., Stimpson, B., Stead, D. (1999): Effect of grain size on the initiation and propagation thresholds of stress-induced brittle fractures. Rock Mech. Rock Engng. 32(2), 81–99.

Hazzard, J. F., Young, R. P. (2000): Micromechanical modeling of cracking and failure in brittle rocks. J. Geophys. Res. 105(B7), 16683–16697.

Homand-Etienne, F., Hoxha, D., Shao, J. F. (1998): A continuum damage constitutive law of brittle rocks. Comput. Geotech. 22(2), 135–151.

Kim, M. K, Lade, P. V. (1984): Modelling rock strength in three dimensions. Int. J. Rock Mech. Min. Sci. Geomech. Abstr. 21(1), 21–33.

Kupfer, H. B., Gerstle, K. H. (1973): Behavior of concrete under biaxial stresses. J. Engng. Mech. Div. ASCE 99(EM4), 852–866.

Maso, J. C., Lerau, J. (1980): Mechanical behavior of Darney sandstone (Vosges, France) in biaxial compression. Int. J. Rock Mech. Min. Sci. Geomech. Abstr. 17, 109–115.

Mazars, J., Pijaudier-Cabot, G. (1987): Continuum damage theory – application to concrete. J. Engng. Mech. ASCE 115(2), 345–365.

Myer, L. R., Kemeny, J. M., Zheng, Z., Suarez, R., Ewy, R. T., Cook, N. G. W. (1992): Extensile cracking in porous rock under differential compressive stress. Appl. Mech. Rev. 45, 263–280.

Nemat-Nasser, S., Hori, M. (1993): Micromechanics: overall properties of heterogeneous materials. North-Holland, Amsterdam.

Ortiz, M. (1988): Microcrack coalescence and macroscopic crack growth initiation in brittle solids. Int. J. Solids Struct. 24, 231–250.

Ostoja-Starzewski, M. (1993): Random fields and processes in mechanics of granular materials. Mech. Mater. 16(1–2), 55–64.

Potyondy, D. O., Cundall, P. A., Lee, C. A. (1996): Modeling rock using bonded assemblies of circular particles. Proc., 2nd North American Rock Mechanics Symposium, NARMS'96, 1996, 1937.

Tang, C. A. (1997): Numerical simulation of progressive rock failure and associated seismicity. Int. J. Rock Mech. Min. Sci. 34(2), 249–261.

Tang, C. A., Kaiser, P. K. (1998): Numerical simulation of cumulative damage and seismic energy release during brittle rock failure, part I: Fundamentals. Int. J. Rock Mech. Min. Sci. 35, 113–121.

Tang, C. A., Liu, H., Lee, P. K. K., Tsui, Y., Tham, L. G. (2000): Numerical studies of the influence of microstructure of rock failure in uniaxial compression, part II: Effect of heterogeneity. Int. J. Rock Mech. Min. Sci. 37, 555–569.

Van Mier, J. G. M. (1997): Fracture processes of concrete: assessment of material parameters for fracture models. CRC Press, Inc, Boca Raton, Florida, 3–5.

Zhu, W. C., Teng, J. G., Tang, C. A. (2002): Mesomechanical model for concrete, part I: Model development. Research Report of Department of Civil and Structural Engineering, The Hong Kong Polytechnic University.

Appendix Notation

The following symbols are used in this paper:

b	ratio of displacements applied in the horizontal and vertical directions
B	brittleness index
D	damage variable
E, E_0	damaged and undamaged (initial) elastic moduli of element
f_{c0}, f_{t0}	compressive and tensile strengths, respectively, of element
f_{cr}, f_{tr}	residual compressive and tensile strengths, respectively, of element
$f(u)$	probability density function of Weibull distribution
m	homogeneity index, shape parameter of Weibull distribution
n	power of the power function indicating the post-peak softening law
u	parameter of elements that conforms to Weibull distribution, such as elastic modulus and strength
u_0	scale parameter of Weibull distribution
u_x, u_y	displacement applied in the horizontal and vertical directions of specimen
ϵ	strain
ε_0	strain at peak stress

$\varepsilon_1, \varepsilon_2, \varepsilon_3$	principal strain
ε_{c0}	strain at the peak compressive stress
ε_{cr}	maximum compressive strain at the residual compressive strength
ε_{t0}	strain at the peak tensile stress
ε_{tr}	maximum tensile strain at the residual tensile strength
ε_{tu}	ultimate tensile strain
ϕ	internal friction angle
η	ultimate tensile strain coefficient
λ	residual strength coefficient
μ	Poisson's ratio
σ	stress
σ_x, σ_y	stresses applied in horizontal and vertical directions of specimen
σ_1, σ_2, σ_3	principal stress

Authors' address: Dr. Wancheng Zhu, Center for Rock Instability and Seismicity Research, Box 138, Northeastern University, Shenyang, 110004, P.R. China; e-mail: wanchengzhu@263.net; crisr@mail.neu.edu.cn